

Modeling and measuring the nocturnal drainage flow in a high-elevation, subalpine forest with complex terrain

Chuixiang Yi,¹ Russell K. Monson,¹ Zhiqiang Zhai,² Dean E. Anderson,³ Brian Lamb,⁴ Gene Allwine,⁴ Andrew A. Turnipseed,^{1,5} and Sean P. Burns¹

Received 27 May 2005; revised 17 August 2005; accepted 1 September 2005; published 16 November 2005.

[1] The nocturnal drainage flow of air causes significant uncertainty in ecosystem CO₂, H₂O, and energy budgets determined with the eddy covariance measurement approach. In this study, we examined the magnitude, nature, and dynamics of the nocturnal drainage flow in a subalpine forest ecosystem with complex terrain. We used an experimental approach involving four towers, each with vertical profiling of wind speed to measure the magnitude of drainage flows and dynamics in their occurrence. We developed an analytical drainage flow model, constrained with measurements of canopy structure and SF₆ diffusion, to help us interpret the tower profile results. Model predictions were in good agreement with observed profiles of wind speed, leaf area density, and wind drag coefficient. Using theory, we showed that this one-dimensional model is reduced to the widely used exponential wind profile model under conditions where vertical leaf area density and drag coefficient are uniformly distributed. We used the model for stability analysis, which predicted the presence of a very stable layer near the height of maximum leaf area density. This stable layer acts as a flow impediment, minimizing vertical dispersion between the subcanopy air space and the atmosphere above the canopy. The prediction is consistent with the results of SF₆ diffusion observations that showed minimal vertical dispersion of nighttime, subcanopy drainage flows. The stable within-canopy air layer coincided with the height of maximum wake-to-shear production ratio. We concluded that nighttime drainage flows are restricted to a relatively shallow layer of air beneath the canopy, with little vertical mixing across a relatively long horizontal fetch. Insight into the horizontal and vertical structure of the drainage flow is crucial for understanding the magnitude and dynamics of the mean advective CO₂ flux that becomes significant during stable nighttime conditions and are typically missed during measurement of the turbulent CO₂ flux. The model and interpretation provided in this study should lead to research strategies for the measurement of these advective fluxes and their inclusion in the overall mass balance for CO₂ at this site with complex terrain.

Citation: Yi, C., R. K. Monson, Z. Zhai, D. E. Anderson, B. Lamb, G. Allwine, A. A. Turnipseed, and S. P. Burns (2005), Modeling and measuring the nocturnal drainage flow in a high-elevation, subalpine forest with complex terrain, *J. Geophys. Res.*, *110*, D22303, doi:10.1029/2005JD006282.

1. Introduction

[2] Eddy covariance tower systems have become the tool of choice for measurement of trace gas and energy exchange between vegetation and the atmosphere [Baldocchi *et al.*,

2000, 2001]. However, when this technique is applied to ecosystems with complex terrain, and for which calm nights are frequent, significant uncertainties can occur. The sensors on the tower above the canopy cannot properly account for the horizontal flows that carry scalars and energy beneath the canopy, the so-called advective flux component [Goulden *et al.*, 1996; Baldocchi *et al.*, 2000; Yi *et al.*, 2000; Aubinet *et al.*, 2003; Staebler and Fitzjarrald, 2004; Feigenwinter *et al.*, 2004; Turnipseed *et al.*, 2003, 2004; Marcolla *et al.*, 2005; Aubinet *et al.*, 2005]. One of the primary causes of advective fluxes is gravitationally induced drainage flows that are especially prevalent in mountain ecosystems. Addition of these mean fluxes to the turbulent flux budget is required to achieve accurate estimates of the total surface-atmosphere exchange of CO₂ and H₂O. In regions of complex topography, which are also among the most important for determining regional and

¹Department of Ecology and Evolutionary Biology, University of Colorado, Boulder, Colorado, USA.

²Department of Civil, Environmental, and Architectural Engineering, University of Colorado, Boulder, Colorado, USA.

³Water Resources Discipline, U.S. Geological Survey, Lakewood, Colorado, USA.

⁴Laboratory for Atmospheric Research, Washington State University, Pullman, Washington, USA.

⁵Now at Atmospheric Chemistry Division, National Center for Atmospheric Research, Boulder, Colorado, USA.

global carbon and water budgets [Barry, 1993; Schimel *et al.*, 2002], the characterization of drainage flows and their associated advective fluxes is especially important.

[3] One line of evidence for the occurrence of drainage flows is the within canopy, S-shaped, wind profile that has been widely observed [Fons, 1940; Allen, 1968; Bergen, 1971; Oliver, 1971; Landsberg and James, 1971; Shaw, 1977; Lalic and Mihailovic, 2002; Turnipseed *et al.*, 2003]. The S-shaped profile refers to a second wind maximum that is often observed within the trunk space of forests and a minimum wind speed in the region of greatest foliage density [Shaw, 1977]. The second wind maximum is likely due to the combined effect of local drainage flows that can achieve relatively high speeds in the lower region of the canopy (D.E. Anderson *et al.*, Mean advective flux of CO₂ in a high elevation subalpine forest during nocturnal conditions, submitted to *Agricultural and Forest Meteorology*, 2005, hereinafter referred to as Anderson *et al.*, submitted manuscript, 2005), and resistance to the mean wind flow that can reduce wind speeds in the region of the canopy with high leaf area density [Massman, 1997; Massman and Weil, 1999; Mohan and Tiwari, 2004; Poggi *et al.*, 2004]. The factors that most determine the potential for drainage flows are terrain slope and nocturnal radiative cooling of the slope surface [Fleagle, 1950; Manins and Sawford, 1979; Doran and Horst, 1981; Mahrt, 1982]. Although past modeling efforts have replicated local drainage flows across sloped terrain [Mahrt, 1982], to our knowledge, no analytical mathematical model has yet predicted the second wind maxima within the context of the entire vertical wind profile. It would be of great benefit to have such a model as its use would move us closer to being able to close scalar and energy budgets for both modeled and measured flux footprints. It would also provide us with even better tools for modeling the processes of scalar and energy fluxes, and thus producing greater accuracy in our predictions of the effects of environmental change on ecosystem biogeochemical cycles.

[4] Our past observations of wind flow patterns at the Niwot Ridge Ameriflux site have revealed the presence of the secondary wind maximum, especially during nights with high atmospheric stability [Turnipseed *et al.*, 2003]. We initially attributed the near-surface maximum as being due to nighttime drainage flows. In a subsequent study, we used an array of four towers, each with vertical profiling of CO₂ and, at least, two-dimensional wind speed to estimate the magnitude and dynamics of horizontal mean advective CO₂ fluxes (Anderson *et al.*, submitted manuscript, 2005). In the current study, we continued analysis of the drainage flow patterns using the four-tower experimental design. In order to interpret our observations, we developed a one-dimensional analytical model that is able to predict the S-shaped wind profile. We constrained the model with observations of forest canopy structure, including detailed observations on the vertical distribution of leaf area density, and we validated some of the model predictions using an SF₆ release experiment. Finally, we tested the analytical model against a numerical model developed with computational fluid dynamics (CFD) techniques; the latter model represents a more detailed, mechanistic model. Overall, our aim was to provide more insight into the dynamics and causes of drainage flows in this ecosystem, and prepare a

means of ultimately assessing the effect of bias in the mean horizontal and vertical flux components on the overall mass balance for CO₂ at the study site.

2. Measurements

2.1. Study Site

[5] The studies were conducted at the Niwot Ridge Ameriflux site located in a subalpine forest ecosystem in the Rocky Mountains of Colorado (40°1'58"N; 105°32'47"W, 3050 m elevation), approximately 25 km west of Boulder and 8 km east of the Continental Divide. The terrain of the site has a slope of approximately 5°–7° within 400 m in the east-west direction. Detailed maps showing the site topography have been presented in past papers [Turnipseed *et al.*, 2003, 2004]. Predominant winds are from the west [Brazel and Brazel, 1983], flowing downslope. Summertime meteorology produces valley-mountain airflows, with thermal-induced, near-surface upslope winds from the east occurring on many afternoons. Nighttime flow is nearly always from the west, and is often katabatic (downslope drainage). The surrounding subalpine forest is ~100 years old, having recovered from clear-cut logging. Very little understory canopy is present due to the thin, often dry soils at the site. Other details for the site can be found in Monson *et al.* [2002] and Turnipseed *et al.* [2002].

2.2. Tower Profile and Eddy Covariance Measurements

[6] A multiple-tower observing system was employed which is capable of measuring eddy fluxes and vertical profiles of the mixing ratios of CO₂, H₂O, wind speed and wind direction. This system consists of four towers: ET (east tower); WT (west tower); NT (north tower) and ST (south tower) (Anderson *et al.*, submitted manuscript, 2005). The ET and WT towers are located 150 m apart and are oriented on a west-east (240°–60°) transect. The NT and ST towers are 150 m apart along the 330°–150° transect. Thus the four towers form the vertices of a diamond, with the west-east points of the diamond aligned along the westerly wind vector known to dominate nighttime flows. Eddy covariance fluxes of CO₂, water vapor and sensible heat were measured on the two west-to-east aligned towers. The ET tower measurement height was 21.5 m and the WT tower measurement height was 33 m. Vertical profiles of scalar mixing ratios, wind speed and wind direction were measured at five levels on the ET and WT towers (1, 3, 6, 10, and 21.5 m on ET tower; 1, 3, 6, 10, and 33 m on WT tower), and at two levels on the two shorter towers (1, 6 m on NT and ST towers). Wind speed and direction were measured with at least two-dimensional, and at several heights three-dimensional, sonic anemometers. The instrumentation, calibration scheme and flux calculation methodology have been described in detail by Anderson *et al.* (submitted manuscript, 2005) and Turnipseed *et al.* [2002, 2003, 2004].

2.3. Leaf Area Density Measurements

[7] Canopy structure was studied in sixteen 10 × 10 m plots, eight directly east and eight directly west of the ET flux tower. The first plot was established at 50 m east or

50 m west of the tower, with subsequent plots established at 20 m intervals. Each tree greater than 1 m in height was measured in all plots (total of 839 trees) for diameter at breast height, height to crown and maximum diameter of crown (typically at the base of the crown) in the N-S and E-W perpendicular coordinates, and total tree height. A separate survey was done of 90 representative trees (30 lodgepole pines, 30 subalpine firs, and 30 Engelmann spruces) in the plots, evaluating diameter at breast height against number of branches in the upper, middle and lower third of the trees, using binoculars to count branches. We found this approach to be accurate to within 10% when checked against a subset of ten trees accessible by canopy access towers at the site; the open nature of the forest, and thin nature of the tree crowns also facilitates accurate viewing with binoculars. Linear regression models predicted 37–54%, 6–24%, and 1–30% of the variance in branch number by diameter at breast height in the top, middle and bottom sections of the trees, respectively. Representative branches from the upper, middle and lower third of the crown in 30 trees equally distributed among each of the three dominant tree species were cut at their intersection with the bole and measured for total needle dry biomass. Needle mass was converted to needle area using a regression constructed from separate analyses of sun and shade needles in 10 trees from each of the three species. Needle areas were determined with the water immersion method described by *Chen et al.* [1997]. From knowledge of needle area per branch, branch number per unit bole diameter, average branch length in the top, middle and bottom thirds of the canopy, and total canopy height and diameter (average diameter of the east-to-west and north-to-south crown diameter measurements), we estimated the average leaf area index (LAI) in 10 cm, concentric circles for each vertical third of the canopy for each of the 839 trees. We assumed that the vertical distribution of LAI in each third of the canopy decreased linearly from the bottom to the top in 1 m thick layers. From these calculations, we were able to estimate the leaf area density (leaf area per unit volume) for each 1 m thick vertical layer of the crown of each tree. The leaf area density was summed for all trees in a plot for each vertical layer between the ground and 16 m (the maximum height of the canopy) and divided by the total area of the plot to provide a vertical profile of leaf area density for the entire plot.

2.4. SF₆ Experiments

[8] Sulfur hexafluoride (SF₆) tracer experiments were conducted in July 2001 and 2002. In 2001, SF₆ was released continuously at a steady rate from a point source located at 0.2 m above the forest floor approximately 50 m upslope from the WT tower. In 2002, SF₆ was released from a 200 m line source deployed across the slope at 0.2 m height and 50 m upslope from the WT tower. Total release rates were controlled with a mass flow controller, and measurements from the individual capillary restrictors (every 3 m along the line) were made from approximately 1/3 of the points during each test day. A fast response, continuous SF₆ analyzer was operated with the existing CO₂ ambient profiler system to measure SF₆ concentrations at 14 locations on the towers (ET, WT, ST, NT) in 2001 and 2002. The profiler sequentially samples for 30 s at each position and the measured

concentrations are combined into 30 minute averages. The analyzer was calibrated using certified commercial standards (5% accuracy) during each test day. In this paper we only report the results from a single SF₆ release during August 2002; this was a period when all of the release and detection instruments appeared to be functioning at optimal levels, atmospheric stability was high, and the observed drainage flows were strong.

3. Theory

[9] For simplicity, the atmosphere is assumed to be stable, incompressible and inviscid. Drainage flow is assumed to develop over a constant slope with angle α . The coordinate system used is Cartesian, with x in the direction of the mean downslope wind, and z normal to the slope. The canopy structure is assumed to be horizontally uniform but varies in the vertical coordinate. No vertical motion and horizontal static pressure gradient are considered, and Coriolis acceleration is neglected. For the steady state condition, drainage flow is governed by [*Wilson and Shaw, 1977; Mahrt, 1982*]:

$$-\frac{\overline{u'w'}}{\partial z} - g \frac{\Delta\theta}{\theta_0} \sin \alpha = c_D(z)\ell(z)u^2(z), \quad (1)$$

where $-\overline{u'w'}$ is the average shear stress, g is the acceleration due to gravity, θ_0 is the ambient potential temperature (in this case taken at 21.5 m height and the influence of moisture on buoyancy is neglected), $\Delta\theta = \theta - \theta_0$ is the deficit of potential temperature in the drainage flow (where θ is the potential temperature of the drainage flow), $\ell(z)$ is the plant area density facing the mean wind (defined as the frontal area of individual elements per unit volume of canopy), $c_D(z) = C_D(z)/p(z)$ is the effective drag coefficient of plant elements subject to a shelter factor $p(z)$ within the canopy [*Massman, 1997; Massman and Weil, 1999*], $C_D(z)$ is the foliage drag coefficient, and $u(z)$ is the average mean wind velocity. The drag coefficient within the canopy is defined according to *Mahrt et al.* [2000] as

$$c_D(z) = \frac{u_*^2(z)}{u^2(z)}. \quad (2)$$

where $u_*(z)$ is the friction velocity within the canopy and is related to the shear stress as

$$-\overline{u'w'} = u_*^2(z). \quad (3)$$

After substitution, equation (1) becomes

$$\frac{\partial(c_D(z)u^2(z))}{\partial z} - c_D(z)u^2(z)\ell(z) = g \frac{\Delta\theta}{\theta_0} \sin \alpha. \quad (4)$$

The cumulative leaf area per unit ground area below height z is defined as

$$L(z) = \int_0^z \ell(z') dz'. \quad (5)$$

Multiplying both sides of (4) by $e^{-L(z)}$ and integrating from height z within the canopy to the top of the canopy h , we obtain

$$u^\pm(z) = \pm \left(e^{-(LAI-L(z))} \frac{c_D^h}{c_D(z)} u_h^2 - g \frac{\Delta\theta \sin \alpha}{\theta_0 c_D(z)} \int_z^h e^{-(L(z')-L(z))} dz' \right)^{\frac{1}{2}}, \quad (6)$$

where $L(h) = LAI$ (the leaf area index), c_D^h and u_h are the respective drag coefficient and mean wind speed at the top of the canopy. Equation (6), is to our knowledge, the first analytical solution to the drainage flow problem inside a forest. Equation (6) retains the “driving” force of gravity and ‘resistive’ force of canopy shear that govern the drainage flow and were originally expressed in equation (1). The solution in equation (6) covers the situations of downslope $[u^+(z)]$ and upslope $[u^-(z)]$ wind speed. At our study site, the steady state upslope flow $[u^-(z)]$ is clearly restricted to daytime periods, and therefore will not be discussed further in this paper. Hereafter, $u(z)$ will refer solely to downslope wind speed $[u^+(z)]$, and in our consideration will be restricted to nighttime periods.

[10] Prediction of the Reynolds stress, $-\overline{u'w'}$, profile within a canopy is important with regard to understanding the complex interactions between wind flow and canopy structure [Shaw, 1977]. Several complicated higher-order closure models have been developed [e.g. Wilson and Shaw, 1977; Katul and Albertson, 1998; Massman and Weil, 1999]. A simple Reynolds stress model can be derived using our parameterization scheme. The drag force density, $c_D(z)u^2(z)$, on the right hand side of equation (1) can be replaced through equations (2) and (3) by the Reynolds stress. Thus equation (1) becomes

$$-\frac{\partial \overline{u'w'}}{\partial z} + \ell(z) \overline{u'w'} = g \frac{\Delta\theta}{\theta_0} \sin \alpha. \quad (7)$$

When we repeat a similar procedure in the derivation of equation (6), we obtain:

$$-\overline{u'w'}(z) = -\overline{u'w'}(h) e^{-(LAI-L(z))} - g \frac{\Delta\theta}{\theta_0} \sin \alpha \int_z^h e^{-(L(z')-L(z))} dz', \quad (8)$$

where $\overline{u'w'}(h)$ is the Reynolds stress at the top of canopy. If the terrain is flat, the dimensionless Reynolds stress profile becomes:

$$\frac{-\overline{u'w'}(z)}{u_*^2(h)} = e^{-(LAI-L(z))}, \quad (9)$$

where $u_*^2(h) = -\overline{u'w'}(h)$. The relative Reynolds stress profile is determined uniquely by the function $e^{-(LAI-L(z))}$. We refer to this function as a ‘canopy buffer function’ because it

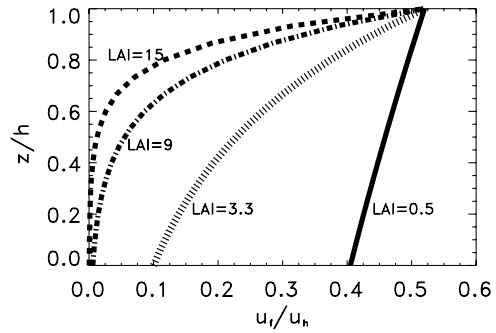


Figure 1. Dependence of slope-independent component of canopy wind profile on LAI predicted by equation (11) (with $c_D = 0.11$, $c_D^h = 0.03$, and $u^h = 2.93 \text{ m s}^{-1}$).

reflects the manner in which canopy structure influences wind flow dynamics within the canopy.

4. Results

4.1. Application of the Model to a Forest Canopy With Simple Structure

[11] As an example of the model, we chose the simple case in which the vegetation has a uniform vertical distribution of leaf area ($\ell(z) = \ell = \text{cons.}$) and drag coefficient ($c_D(z) = c_D = \text{cons.}$). With these assumptions, equation (6) is reduced to

$$u(z) = \left(\frac{c_D^h u_h^2}{c_D} e^{-LAI(1-\frac{z}{h})} - \frac{gh\Delta\theta \sin \alpha}{\theta_0 LAI c_D} \left(1 - e^{-LAI(1-\frac{z}{h})} \right) \right)^{\frac{1}{2}}, \quad (10)$$

where we used

$$\frac{L(z)}{L(h)} = \frac{\int_0^z \ell(z') dz'}{\int_0^h \ell(z') dz'} = \frac{z}{h}, \text{ and } \ell(z) = \frac{LAI}{h}.$$

We can partition equation (10) into slope-independent and slope-dependent components. The slope-independent component can be written as:

$$u_f(z) = \sqrt{\frac{c_D^h}{c_D}} u_h e^{-\frac{LAI}{2}(1-\frac{z}{h})}. \quad (11)$$

This is the widely used exponential model for wind profile within a canopy [Inoue, 1963; Cionco, 1965; Cowan, 1968; Cionco, 1972; Raupach and Thom, 1981; Albini, 1981; Wilson et al., 1982; Massman, 1987; Macdonald, 2000; Mohan and Tiwari, 2004]. The dependence of the slope-independent component on LAI is illustrated in Figure 1. The prediction from the model clearly reflects the overall influence of the canopy foliar density that resists mean wind flow, and reduces wind speed to extremely low values at high foliar densities. Using the same assumptions, the slope-dependent component can be written as

$$u_g(z) = \sqrt{-\frac{gh\Delta\theta \sin \alpha}{\theta_0 LAI c_D} \left(1 - e^{-LAI(1-\frac{z}{h})} \right)}. \quad (12)$$

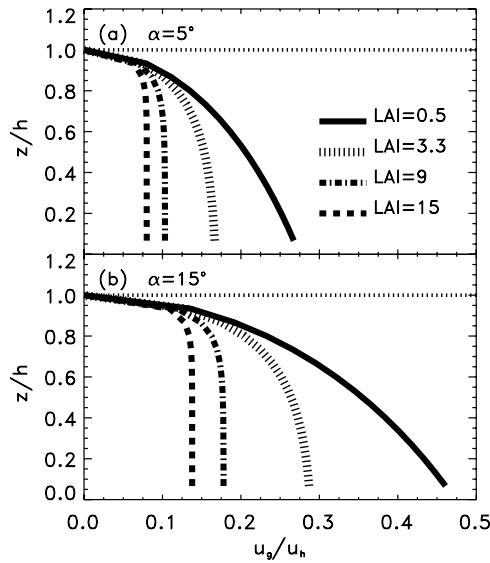


Figure 2. Dependence of slope-dependent component of canopy wind profile on LAI predicted by equation (12) with two respective slopes: (a) $\alpha = 5^\circ$ and (b) $\alpha = 15^\circ$. The values of the rest of the parameters in equation (12) are specified as $c_D = 0.11$, $\Delta\theta = -2$ K, and $\theta_0 = 283$ K.

Equation (12) has a gravity-dependent driver that enhances wind speed in the lower part of canopy, as shown in Figure 2. Foliar density impedes the gravitational flow, however, causing wind speed to decrease with increasing of LAI, in the same manner as that for the slope-independent component.

[12] Under this uniform canopy structure condition, the Reynolds stress profile (equation (8)) becomes:

$$-\overline{u'w'}(z) = -\overline{u'w'}(h)e^{-\text{LAI}(1-\hat{\tau})} - \frac{gh\Delta\theta \sin \alpha}{\theta_0 \text{LAI}} \left(1 - e^{-\text{LAI}(1-\hat{\tau})}\right). \quad (13)$$

The LAI dependence of the Reynolds stress is similar to that of the mean wind speed as shown in Figures 1 and 2.

4.2. Application of the Model to the Niwot Ridge Canopy

[13] We applied equation (6) to the Niwot Ridge forest canopy to derive the vertical profile in canopy drag and to partition the influences of the slope-independent and slope-dependent components on the downslope drainage flow velocity. In this derivation, we used the observed mean wind speed profile from two of the four towers (Figure 3). In using equation (6), the value for u_h was taken from the analysis shown in Figure 3 as 2.93 m s^{-1} ; values for $u(z)$ were taken as the measured mean wind values at the respective heights reported in Figure 3. The upper part of the profile $u(z)$ (i.e., above 10 m) was calculated by the semilogarithmic wind profile:

$$u(z) = \frac{u_*}{k} \ln\left(\frac{z-d}{z_0}\right). \quad (14)$$

using von Karman's constant (k) as 0.4 and u_* as $0.6 \text{ (m s}^{-1}\text{)}$. The displacement height (d) and roughness

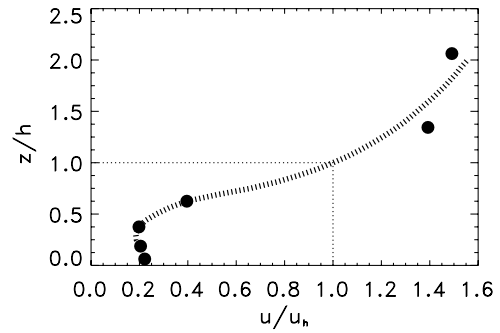


Figure 3. Averaged wind profile (circles) over nights ($N = 2556$) in 2002. Points at level 1, 3, 6, 10, and 33 m were measured on the west tower (WT), the point at level 21.5 m was measured on the east tower (ET). Data were only included that were available for all six levels within a single averaging period. Error bars for all points were smaller than the symbols. The line with horizontal dashes is a smoothed curve. The upper part of the line was calculated by the semilogarithmic wind profile as described by *Turnipseed et al.* [2003].

length (z_0) under near-neutral atmospheric stability were taken as 7.8 m and 1.16 m, respectively, which represent measured values for the site [*Turnipseed et al.*, 2003]. Although the semilogarithmic law is probably invalid under many conditions in the roughness sublayer [e.g., *Raupach and Thom*, 1981], it is the only tool we have available at the present time for smoothing the wind profile; it has limitations in this analysis, which will be discussed shortly.

[14] The drag coefficient profile was derived by equation (6) with $\Delta\theta = -2$ K, $\theta_0 = 283$ K, and slope $\alpha = 5^\circ$ (Figure 4). *Mahrt et al.* [2001] have shown that the surface

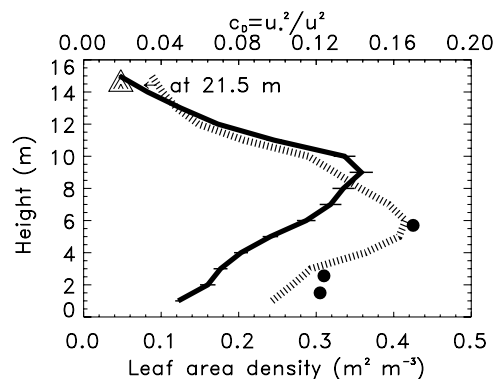


Figure 4. The leaf area density profile (solid line) observed and drag coefficient profile (line with horizontal dashes) derived by equation (6). The circles and triangle were the average drag coefficients calculated by equation (2) from the half-hour eddy covariance data at 1.5, 2.56, 5.7, and 21.5 m. The data used in the averages at 1.5, 2.56 and 21.5 m occurred in the same averaging periods during the nights of 2002 ($N = 1798$), while the data used at 5.7 m were in the nights of 2003 ($N = 2603$). The surface drag coefficient observed at 21.5 m (triangle) is close to the modeled values at the top of canopy. The horizontal error bars indicate ± 1 standard error of the mean leaf area density.

drag coefficient is independent of stability as wind speed exceeds 2 m s^{-1} for forests. The value $c_D^h = 0.03$ (for $u_h = 2.93 \text{ m s}^{-1}$) is close to the range of values observed by *Mahrt et al.* [2001] in representative forests. Drag coefficients (circles and triangle in Figure 4) were obtained in a two-step calculation: half-hour values were first calculated by equation (2) and then averaged for each level over the entire nighttime period. The order of calculation will influence the estimated values due to the nonlinearity in equation (2). The records with small stress ($u_* < 0.01 \text{ m s}^{-1}$) and weak wind speeds ($< 0.10 \text{ m s}^{-1}$) were screened out due to potential errors [*Mahrt et al.*, 2000]. The data used in the averages at 1.5, 2.56 and 21.5 m occurred in the same hours in the nights of 2002 ($N = 1798$). However, the data used for the level at 5.7 m were in the nights of 2003 ($N = 2603$). Although sampling times for level 5.7 m were not the same as those for the other heights, the mean values appear to fall within the expected portion of the graph, indicating consistent parameter constraint and data population distribution during these two different years. These observed drag coefficient values are within the range 0.12–0.19 of that was observed for a coniferous forest at Lavarone in Italy by *Cescatti and Marcolla* [2004].

[15] The predicted drag coefficient profile is in relatively good agreement with the observed vertical profile in leaf area density (Figure 4). The model, however, predicts a greater proportional decrease in the drag coefficient of the beneath-canopy air space, compared to the decrease in leaf area density. In this canopy, the nature of the leaf area density changes as a function of height in the canopy air space. Above 5 m, canopy elements are mostly represented by needles and branches, whereas below 5 m needle density decreases to relatively low values and the density of canopy elements is mostly reflected in dead, persistent branches (data not shown). It is possible that the stiffness of the dead branches, and their tendency to not flex or move under the force of the airflow, causes them to impose a higher drag on the flow than predicted with traditional foliar drag coefficients.

[16] The components of downslope wind speed $u = \sqrt{u_f^2 + u_g^2}$, where

$$u_f(z) = u_h \sqrt{\frac{c_D^h}{c_D(z)}} e^{-\frac{1}{2}(LAI-L(z))}, \quad (15)$$

$$u_g = \sqrt{-g \frac{\Delta\theta \sin(\alpha)}{\theta_0 c_D(z)} \int_z^h e^{-(L(z')-L(z))} dz'}, \quad (16)$$

are shown in Figure 5a. Gravitational forces (reflected in the slope-dependent component) are more important than the mean wind (reflected in the slope-independent component) in driving the drainage flow between the ground surface and a height approximately 4 m above the ground. The slope-independent component contributes more to the shape of the wind profile above 4 m; this is primarily due to the effect of plant elements impeding the transport of momentum downward to the ground. Overall, both components must be considered to understand the causes of the S-shaped

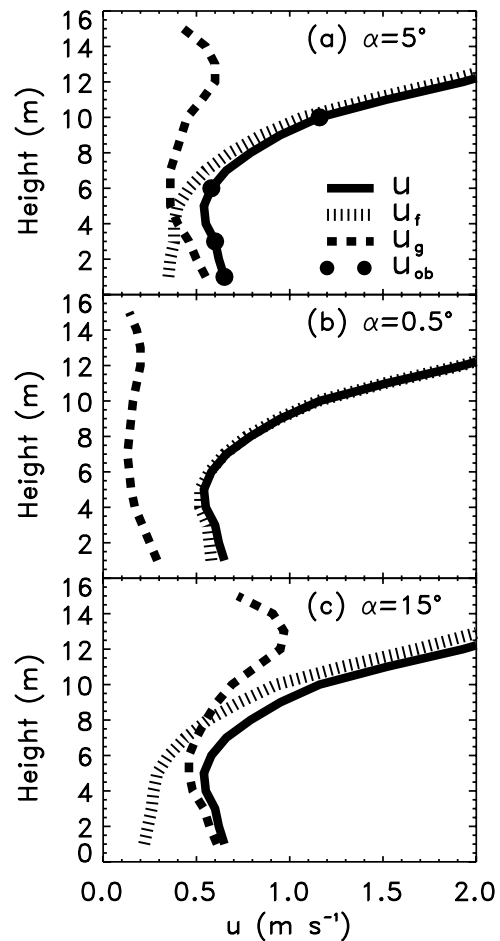


Figure 5. Partitioning of the downslope wind speed $u = \sqrt{u_f^2 + u_g^2}$ (solid line) into a slope-dependent component u_g (line with vertical dashes) and a slope-independent component u_f (line with horizontal dashes) with three respective slopes: (a) $\alpha = 5^\circ$, (b) $\alpha = 0.5^\circ$, and (c) $\alpha = 15^\circ$. The circles are observations as in Figure 3. The profiles of wind speed (solid line) and the leaf area density (solid line in Figure 4) were used as constraints in the partitioning.

wind profile within the canopy. It should be noted that this partitioning is dependent on terrain slope (Figures 5b and 5c). For the case of relatively flat terrain, canopy structure and influences on the mean wind are the major causes for the S-shaped wind profile (Figure 5b). In the case of a terrain slope equal to 15° , the wind profile is determined mainly by the slope-dependent forcings below 8 m (Figure 5c).

[17] The predicted Reynolds stress profile is shown in Figure 6 with data from observations included for comparison. The entire profile is largely controlled by the canopy buffer function. Most of the flow momentum is extracted in a relatively thin layer of the upper canopy. The Reynolds stress in the lower canopy is almost uniform and caused mainly by gravitational flow.

[18] In order to compare our simple model with past higher-order closure models [*Wilson and Shaw*, 1977; *Albini*, 1981] we used equation (9) and the leaf area density data reported by *Shaw* [1977] to calculate the dimensionless

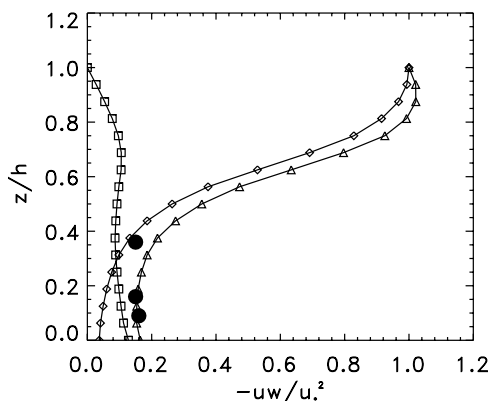


Figure 6. Dimensionless Reynolds stress profile predicted by equation (8): triangles, total Reynolds stress; diamonds, slope-independent component; squares, slope-dependent component; circles, observations. The observed data points were obtained from the same data sets as in Figure 4.

Reynolds stress profile (Figure 7). Predictions of the stress profile using our simple model were similar to those from the Wilson and Shaw (WS) model and in better agreement than other past models.

4.3. Prediction of a Very Stable Air Layer Within the Canopy

[19] The vertical profile of wind speed predicted by equation (6) provides evidence of a layer with relatively low flow between 3 and 6 m above the ground (Figure 3). This layer lies immediately below the layer of maximum leaf area density. We confirmed the existence of the stable layer using measurements of the vertical profile in wind

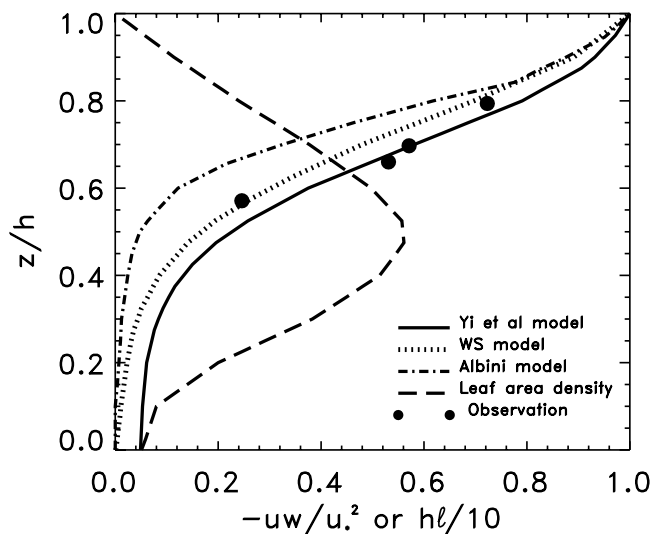


Figure 7. Comparison of dimensionless Reynolds stress profile predicted by present simple model and the higher-order closure models (WS model refers to *Wilson and Shaw* [1977]; Albin model refers to *Albin* [1981]) on the basis of the data reported by *Shaw* [1977]. The canopy height was 2.9 m, and LAI was 3.0 [*Shaw et al.*, 1974].

speed and air temperature (Figure 8). Using the Richardson number (Ri) [*Thom*, 1971] defined as

$$Ri = \frac{g}{\theta_0} \frac{\partial T}{\partial z} \rightarrow \infty$$

with $\partial u/\partial z = 0$ (Figure 8a) and $\partial T/\partial z \neq 0$ (Figure 8b), we observed maximum stability at 6 m when the above-canopy atmosphere was stable ($0.05 \leq (z - d)/L$) and 3 m when the above-canopy atmosphere was neutral ($-0.05 < (z - d)/L < 0.05$). Although the wind speed (Figure 8a) and temperature (Figure 8b) were measured in different summers, the occurrence of stable 30 min observation periods ($\sim 90\%$) and near-neutral 30 min observation periods ($\sim 10\%$) were similar for both years.

[20] We interpret the layer of maximum leaf area density, just above the within-canopy stable layer, to act as a “lid” that minimizes vertical exchange between the lower and upper canopy layers, essentially uncoupling the nighttime near-surface layer from the layers near the top of the canopy. We conducted SF_6 tracer release experiments to confirm this hypothesis. During a 3.5 hour observation period on the night of 8 August 2002 (Figure 9), when atmospheric stability was relatively high, drainage flows were strong (Figure 10), and the SF_6 release line and tower-mounted sensors were well calibrated and working at

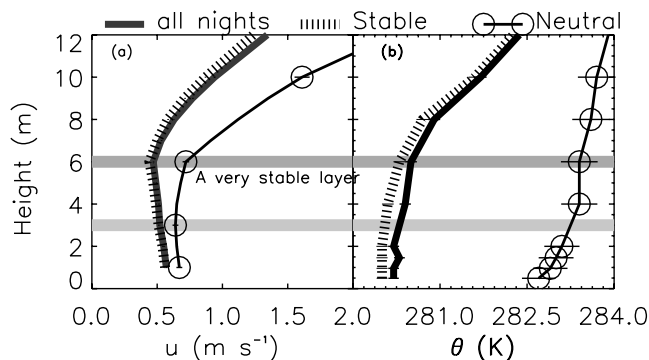


Figure 8. The profiles of average (a) wind speed and (b) temperature during nighttime periods. The data used in Figure 8a represent the average wind speed profile over whole summer nights in 2002; the solid line includes all available data in the summer nights of 2002 ($N = 1213$ for each level), the line with horizontal dashes is for above-canopy stable hours ($N = 1087$, $0.05 \leq (z - d)/L$, L is the Obukhov length measured at $z = 21.5$ m level, $d = 7.8$ m [see *Turnipseed et al.*, 2003]), and the line with circles is for near-neutral hours ($N = 126$, $-0.05 < (z - d)/L < 0.05$). The temperature data used in Figure 8b were measured at levels 0.49, 0.96, 1.46, 2, 4, 6, 8, 10 m by thermocouples in the summer of 2003; the solid line is for all available data in the summer nights ($N = 1425$), the line with horizontal dashes is for stable hours ($N = 1273$, $0.05 \leq (z - d)/L$), and the line with circles is for near-neutral hours ($N = 152$, $-0.05 < (z - d)/L < 0.05$). A very stable layer exists with $\partial u/\partial z \approx 0$ (Figure 8a) and $\partial T/\partial z \neq 0$ (Figure 8b) near the 6 m level (dark gray area) for stable hours and near the 3 m level (light gray area) for near-neutral hours. The horizontal error bars indicate ± 1 standard deviation of the mean.

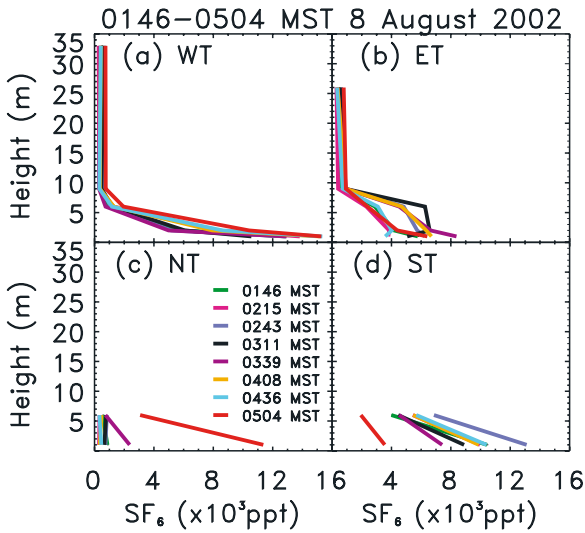


Figure 9. Half-hour average of SF_6 concentrations at four towers during the period 0146–0504 LT on 8 August 2002. During the observation period we observed the typical S-shaped wind profile (see Figure 10) and the mean Obukhov stability was calculated as $\zeta = (z - d)/L \approx 5.87$, indicating highly stable atmospheric conditions above the canopy (at 21.5 m).

optimal performance, we made observations of vertical dispersion at all four observation towers (Figure 9). There was clear sharp stratification among even the lowest observation layers on the WT tower only 50 m downslope from the release line, indicating the presence of a thin downslope flow with little upward mixing. By the time the tracer-laden air reached the lower towers, there was evidence of some vertical mixing to the 6 m layer, but essentially none in the layers above 8 m, even at the lowermost tower, 200 m downslope from the release line. At the south tower (ST) and north tower (NT) we only made observations at the lowest vertical levels; however even at these levels, there was sharp stratification between the lowest and highest levels.

4.4. Wake-to-Shear Production Rate as a Possible Cause of the Within-Canopy Stable Layer

[21] We hypothesized that the stable, within-canopy layer is due to a localized region of high wake-to-shear production ratio. We explored this hypothesis using the analytical model. Ignoring the slope-dependent term in equation (1) we can write

$$\frac{\partial \overline{u'w'}}{\partial z} = -c_D(z)\ell(z)u^2(z) = f_D. \quad (17)$$

Physically, the drag force (form drag) f_D is a direct consequence of noncommutation of differentiation and area averaging over a horizontal plane that intersects numerous plants, producing the pressure force [Wilson and Shaw, 1977; Raupach et al., 1986]. The wake turbulent production rate is the work done by the flow against the form drag and can be written as

$$P_w = -uf_D = -u \frac{\partial \overline{u'w'}}{\partial z}. \quad (18)$$

The shear production rate is usually expressed as

$$P_s = -\overline{u'w'} \frac{\partial u}{\partial z}. \quad (19)$$

The ratio of the wake and shear production rates is therefore

$$\frac{P_w}{P_s} = \frac{-u \frac{\partial \overline{u'w'}}{\partial z}}{-\overline{u'w'} \frac{\partial u}{\partial z}}. \quad (20)$$

Substituting equations (2) and (3) into equation (20), the ratio is reduced to

$$\frac{P_w}{P_s} = \left(\frac{u \partial c_D / \partial z}{c_D \partial u / \partial z} + 2 \right). \quad (21)$$

Thus the ratio can be estimated on the basis of the wind profile presented in Figure 3 and the drag coefficient profile presented in Figure 4. Qualitatively, the vertical gradient of the drag coefficient is almost opposite to that of wind speed. If the wake-to-shear production ratio is physically limited to be positive, then it should be theoretically less than or equal to 2.

[22] The ratio for the upper part of the canopy calculated by equation (21) based on the wind and drag coefficient profiles is shown in Figure 11. Calculated values were indeed less than 2, except in the lowest part of the canopy, where equation (21) may not be valid because $\partial u / \partial z \approx 0$. The maximum wake-to-shear production rate appears near the canopy height of maximum leaf density level rather than near the top of canopy as has been shown in wind tunnel experiments [Raupach et al., 1986]. The relative wake production rate decreases linearly to zero from near the maximum leaf area density level to the top of canopy; following the decrease in leaf area density that occurs in the upper canopy layers of these conically shaped trees. We interpret this pattern as reflecting the fact that wake turbulence is caused by the small-scale pressure gradient associated with canopy elements and hence depends on leaf area density.

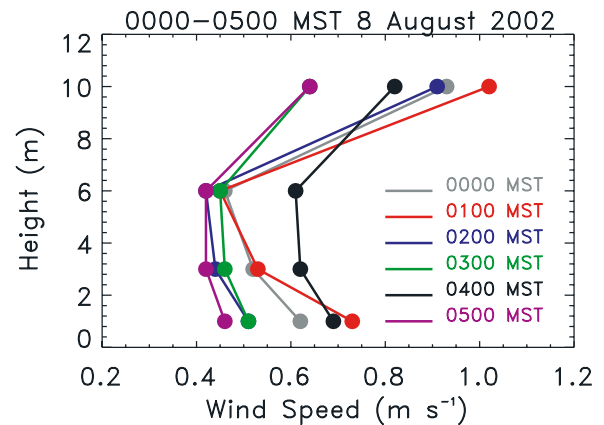


Figure 10. Half-hour average of wind speed at the WT tower during the same period as the SF_6 was observed in Figure 9.

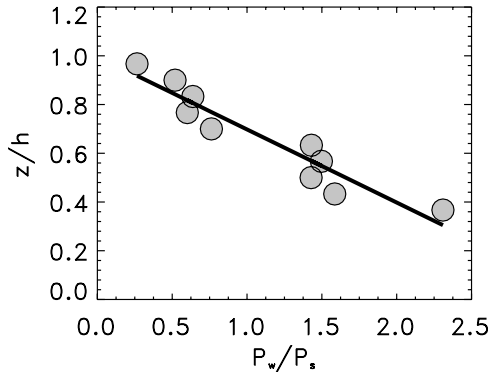


Figure 11. The ratio of the wake and shear production rates calculated from equation (21) based on the wind profile in Figure 3 and drag coefficient profile in Figure 4.

[23] In order to examine the effect of leaf area density on wake production, we applied equations (11) to (21) to the case of a uniform vertical distribution of LAI, which causes equation (21) to become

$$\frac{P_w}{P_s} = \left(\frac{2h\partial c_D/\partial z}{c_D \text{LAI}} + 2 \right). \quad (22)$$

The prediction by equation (22) with the mean values derived from the drag coefficient profile in Figure 4 ($\partial c_D/\partial(z/h) = -0.067$ and $c_D = 0.11$) is shown in Figure 12. Wake-to-shear production rate increases linearly with increasing LAI for $\text{LAI} < 2 \text{ m}^2 \text{ m}^{-2}$, is progressively more limited in its increase for $\text{LAI} \geq 2 \text{ m}^2 \text{ m}^{-2}$, and approaches an asymptote near 2 as $\text{LAI} \rightarrow \infty$.

4.5. Simulations With Computational Fluid Dynamics

[24] To verify the experimental and analytical results, we further simulated airflow within and above the canopy using computational fluid dynamics (CFD) techniques. CFD can predict the spatial and temporal distributions of air pressure, velocity, temperature, humidity, and scalar concentration, as well as turbulence if any, by numerically solving the conservation equations for fluid flows. The present CFD simulation solves the two-dimensional steady state incompressible Reynolds-averaged Navier-Stokes equations of fluid flow, which can be expressed in a Cartesian coordinate system [Patankar, 1980; Anderson *et al.*, 1984] as

$$\frac{\partial U_i}{\partial x_i} = 0, \quad (23)$$

$$U_j \frac{\partial U_i}{\partial x_j} = -\frac{\partial P}{\partial x_i} + \frac{\partial}{\partial x_j} \left((\nu + \nu_t) \frac{\partial U_i}{\partial x_j} \right) - g_i \eta (T - T_\infty) - F_D, \quad (24)$$

$$U_j \frac{\partial T}{\partial x_j} = \frac{\partial}{\partial x_k} \left((\Gamma + \Gamma_t) \frac{\partial T}{\partial x_k} \right) + q_{source} \quad (25)$$

where U_i and U_j are the Reynolds-averaged velocity components in x_i and x_j directions, P is the Reynolds-averaged pressure, T is the Reynolds-averaged air tempera-

ture, ν is the air molecular kinematic viscosity, ν_t is the turbulent “eddy” viscosity, $\Gamma = \nu/\text{Pr}$ is the temperature viscous diffusion coefficient, and $\Gamma_t = \nu_t/\text{Pr}$ is the turbulent viscous diffusion coefficient, where Pr is the Prandtl number, and q_{source} is the energy source in the fluid. The term $-g_i \eta (T - T_\infty)$ represents the buoyancy force on fluid flow, where g_i is the gravity acceleration in i direction, η is the thermal expansion coefficient of air, and T_∞ is the reference temperature. F_D in equation (24) stands for the drag force (pressure drop) exerted by plant elements,

$$F_D = \frac{1}{2} K_r u^2, \quad (26)$$

where K_r is the resistance coefficient, which can be related to the porosity by an empirical relationship given by Hoener [1965]

$$K_r = \frac{1}{2} \left[\frac{3}{2\beta} - 1 \right]^2 \quad (27)$$

where β is the porosity that can be determined from the leaf area density and drag coefficient profiles by assuming that the drag force term in equation (26) is equal to that in equation (1).

[25] The turbulent “eddy” viscosity ν_t can be determined through various turbulence models. In this study we used a renormalized group k - ϵ turbulence model [Yakhot *et al.*, 1992], which generally has better accuracy and numerical stability than the “standard” k - ϵ model [Launder and Spalding, 1974]. Equations (23)–(25) with the turbulence model are not mathematically closed until boundary conditions are specified for the flow field. The boundary conditions involved in this study include (1) inflow, upwind wind profile specified with the semilogarithmic law and $T = 7^\circ\text{C}$; (2) outflow, leeward and sky with fixed static pressure of 1 atm; (3) ground, nonslip condition with negative heat flux of -20 W m^{-2} ; (4) internal objects (plants) with resistance and heat, the resistance is specified according to equation (26) and the long-wave radiation from the plants is specified to linearly decrease from 63 W m^{-2} at the top

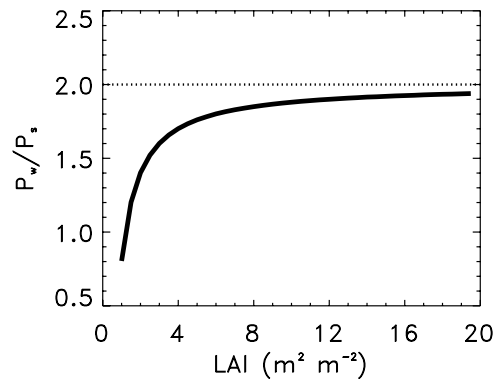


Figure 12. The dependence of the ratio of the wake and shear production rates on LAI. The curve is predicted by equation (22) for given $\partial c_D/\partial(z/h) = -0.06$ (mean value derived from the drag coefficient profile in Figure 4) and $c_D = 0.11$.

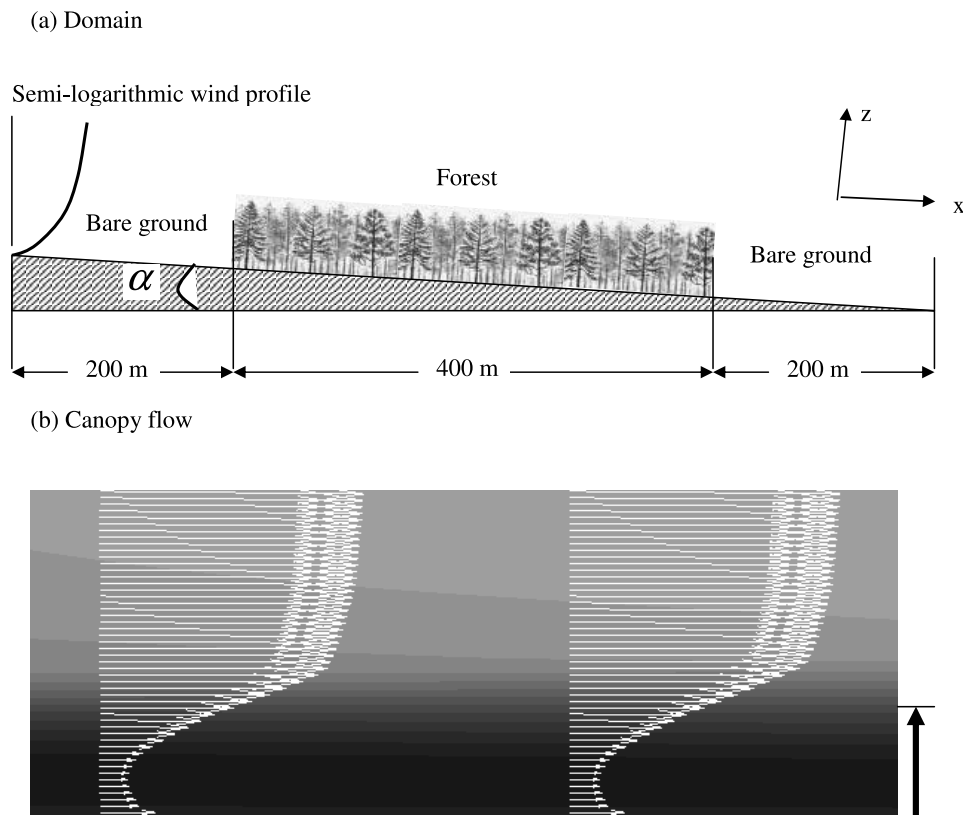


Figure 13. (a) Domain and (b) simulated two-dimensional canopy flow by the renormalized group $k\text{-}\epsilon$ turbulence model. The drag coefficient profile derived from the analytical model and the leaf area density profile in Figure 4 were used as inputs in the numerical model. In this simulation, slope $\alpha = 5^\circ$, temperature deficit $\Delta T = -6^\circ\text{C}$, and details for the boundary conditions are described in the text. The flow field shown in Figure 13b is a snapshot of simulated results taken near the middle of the domain. The different gray shading in the background in Figure 13b indicates the wind speed contours. The white arrows represent wind vectors that indicate wind direction and magnitude of wind speed. The total height of the domain in the simulation is 50 m. The dark arrow on right-hand side of Figure 13b shows the modeled canopy height. Note the minimum wind speed that is reached at the approximate height of the midcanopy layer of maximum LAI and the secondary maximum wind speed that is reached in the lower canopy trunk space.

layer of the canopy to zero at the middle of canopy (i.e., the stable situation specified by *Siqueira and Katul* [2002]).

[26] The flow-governing equations (23)–(25) with boundary conditions are highly nonlinear and self-coupled, which renders them impossible for analytical solution for most real cases. Hence, using CFD, we solve the equations by dividing the spatial continuum into a finite number of discrete cells and discretizing the equations using the finite volume method (FVM), thus converting them to a set of numerically solvable algebraic equations. An iterative procedure is then used to obtain the solution for each discrete field and equations. More detailed descriptions of CFD are given by *Patankar* [1980] and *Anderson et al.* [1984].

[27] In the present study we used a validated CFD program [*Concentration Heat and Momentum Ltd.*, 1999] to simulate the forest canopy flow. The simulation divides the flow field into $200 \times 200 = 40,000$ cells in $x\text{-}z$ section, which represents one computational node per 4 m in the x coordinate, per 0.15 m in the z coordinate within the canopy volume (0–16 m height), and per 0.56 m in

the z coordinate above the canopy (17–28 m height). The computing time for such a simulation is about 4 hours on a PIII-900 MHz desktop PC. Figure 13 illustrates the computational domain and the calculated velocity vectors and contours within and above the canopy. The secondary wind speed maximum due to drainage flow near ground and minimum wind speed near the canopy level with maximum leaf area density are clear in the CFD-simulated results (Figure 13b). Caution should be taken in interpreting the simulated velocity field in the upper part of the domain (30–50 m) as the possible influence of larger-scale air motions like mountain waves [*Durrant*, 1990; *Turnipseed et al.*, 2004] were not considered in this simulation. Overall, the simulated wind profile within and above the canopy is in excellent agreement with the observations and analytical solution described in previous sections, especially below 10 m (Figure 14). Small differences between the results from the CFD model and observations above the 10 m height probably result from use of the semilogarithmic law to smooth the observational wind profile. This would be

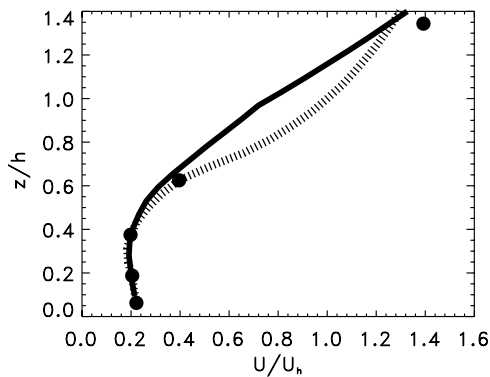


Figure 14. Comparison of the simulated wind profiles from the CFD model (solid line), the analytical solution (equation (6)) (line with horizontal dashes), and observations (circles).

consistent with past studies that have shown the local flux-gradient relationship [Raupach and Thom, 1981] to be inadequate in the roughness sublayer.

[28] Figure 15 shows the two-dimensional canopy flow simulated by the CFD model with the assumption of a uniform vertical distribution of LAI. The exponential canopy wind profile as shown in Figure 1, rather than the S-shaped wind profile, resulted from the uniform distribution condition; this is the same result produced from the analytical solution (see above). The results from the uniform distribution condition also showed the disappearance of the very stable within-canopy air layer. Thus, using this independent modeling approach, we see the clear effect of canopy structure, and its tendency to cause surface drag, on the vertical distribution of the horizontal wind speed and the production of the “super” stable layer within the canopy.

5. Conclusions

[29] The analytical, one-dimensional flow model derived in this study represents a breakthrough in the modeling of the S-shaped canopy wind profile. The model retains the fundamental features of past drainage flow models based on differential equations, including (1) the fact that S shape is determined by the flow resistance properties of canopy structure, i.e., the drag area of plant elements and associated drag coefficient, and (2) that the primary forcing variables

determining flow wind speed near the ground surface are potential temperature deficit and slope angle. Using the analytical model, however, we showed that as height above the ground increases, the shape of the wind profile is progressively more determined by the canopy drag profile, than by the gravitational driving force profile. The one-dimensional model is reduced to the widely used exponential wind profile model under conditions where vertical leaf area density and drag coefficient are uniformly distributed.

[30] Our one-dimensional model successfully predicted the familiar S-shaped canopy wind profile and the Reynolds stress profile in the same manner as considerably more complicated higher-order closure models and, as in the other models, avoided reliance on eddy viscosity (K theory), which often fails in forest canopies. Our model recognizes the drag force as an essential component in describing interactions between plants and air flow, and we express the Reynolds stress by coupling it to the drag force density without introducing phenomenological relations. This is an improvement over past higher-order closure models which introduce phenomenological ‘tuning’ to achieve final closure in the higher-order quantities.

[31] Through two independent modeling approaches, the analytical model and a discretized CFD model, we showed that the heterogeneous vertical distribution of leaf area index produces a stable within-canopy layer of air. The stable layer acts like a lid that minimizes the vertical exchange of mass and momentum below and above the layer. The stable layer appears to be the result of maximum wake production in the region of maximum leaf area density that is characterized by small-scale turbulence and high dissipation rates [Raupach and Shaw, 1982]. The presence and influence of the stable layer is supported by SF₆ diffusion observations. The existence of a stable within-canopy layer leads us to conclude that horizontal mean advective fluxes are restricted to a relatively shallow layer of air beneath the canopy, with little vertical mixing across a relatively long horizontal fetch. Vertical mean advective fluxes are minimal in the subcanopy air space, but originate near the top of the canopy and are significant above the canopy. The vertical structure of these advective fluxes appears to be highly determined by the vertical structure in leaf area density, and its effects on the profile of the horizontal wind speed. With particular reference to the vertical advective flux, our discovery of a very stable layer of air within the canopy has important ramifications

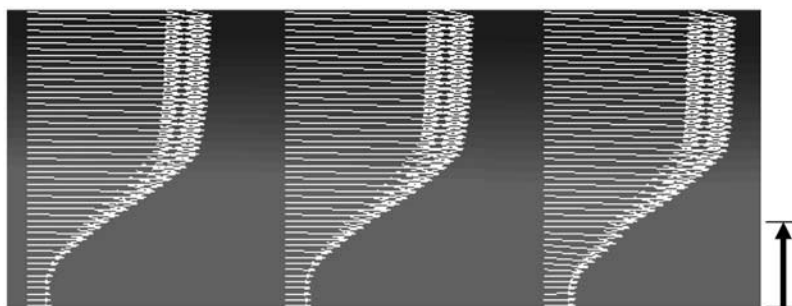


Figure 15. The simulated two-dimensional canopy flow by the renormalized group k - ϵ turbulence model under uniform vegetation condition ($c_D = 0.042$ and $\ell = 0.22 \text{ m}^2 \text{ m}^{-3}$). All other specifications for this simulation are the same as in Figure 13. The symbols are the same as in Figure 13b.

for understanding certain causal relationships. In the past, we reported the existence of a positive bias to the vertical mean wind speed (\bar{w}) in the vicinity of the ET tower at the site [Turnipseed *et al.*, 2003]. Our original hypothesis was that the accumulation of drainage flows at the site could be forcing the flow upward. With knowledge about the within-canopy super stable layer, it would appear that such flows originate in the canopy layers above the region of maximum foliar density, not close to the ground as originally hypothesized. This issue is clearly in need of further investigation.

[32] **Acknowledgments.** This work was financially supported by a grant from the South Central Section of the National Institute for Global Environmental Change (NIGEC) through the U.S. Department of Energy (BER Program) (cooperative agreement DE-FC03-90ER61010) and through funds from the U.S. Department of Energy Terrestrial Carbon Processes Program (TCP) (grant DE-FG02-03ER63637). Any opinions, findings, and conclusions or recommendations expressed in this publication are those of the authors and do not necessarily reflect the views of the DOE. We are grateful for valuable discussions with William J. Massman. The facilities of the University of Colorado Mountain Research Station (MRS) and the support of Bill Bowman (Director of the MRS) and Steve Seibold are gratefully acknowledged. We are grateful for permission by the U.S. Forest Service to conduct the studies in the Roosevelt National Forest.

References

- Albini, F. A. A. (1981), Phenomenological model for wind speed and shear stress profiles in vegetation cover layers, *J. Appl. Meteorol.*, *20*, 1325–1335.
- Allen, L. H., Jr. (1968), Turbulence and wind speed spectra within a Japanese larch plantation, *J. Appl. Meteorol.*, *7*, 73–78.
- Anderson, D. A., J. C. Tannehill, and R. H. Pletcher (1984), *Computational Fluid Mechanics and Heat Transfer*, 599 pp., Taylor and Francis, Philadelphia, Pa.
- Aubinet, M., B. Heinesch, and M. Yernaux (2003), Horizontal and vertical CO₂ advection in a sloping forest, *Boundary Layer Meteorol.*, *108*, 397–417.
- Aubinet, M., et al. (2005), Comparing CO₂ storage and advection conditions at night at different CARBOEUROFLUX sites, *Boundary Layer Meteorol.*, *116*, 63–94.
- Baldocchi, D. D., J. J. Finnigan, K. W. Wilson, U. K. T. Paw, and E. Falge (2000), On measuring net ecosystem carbon exchange in complex terrain over tall vegetation, *Boundary Layer Meteorol.*, *96*, 257–291.
- Baldocchi, D. D., et al. (2001), Fluxnet: A new tool to study the temporal and spatial variability of ecosystem-scale carbon dioxide, water vapor, and energy flux densities, *Bull. Am. Meteorol. Soc.*, *82*, 2415–2434.
- Barry, R. G. (1993), *Mountain Weather and Climate*, 402 pp., Methuen, New York.
- Bergen, J. D. (1971), Vertical profiles of windspeed in a pine stand, *For. Sci.*, *17*, 314–321.
- Brazel, A., and P. Brazel (1983), Summer diurnal wind patterns at Niwot Ridge, CO, *Phys. Geogr.*, *4*, 53–61.
- Cescatti, A., and B. Marcolla (2004), Drag coefficient and turbulence intensity in conifer canopies, *Agric. For. Meteorol.*, *121*, 197–206.
- Chen, J. M., P. M. Rich, S. T. Gower, J. M. Norman, and S. Plummer (1997), Leaf area index of boreal forests: Theory, techniques, and measurements, *J. Geophys. Res.*, *102*, 29,429–29,443.
- Cionco, R. M. (1965), A mathematical model for air flow in a vegetation canopy, *J. Appl. Meteorol.*, *4*, 517–522.
- Cionco, R. M. (1972), A wind-profile index for canopy flow, *Boundary Layer Meteorol.*, *3*, 255–263.
- Concentration Heat and Momentum Ltd. (1999), PHOENICS, version 3.1, London.
- Cowan, I. R. (1968), Mass, heat, and momentum exchange between stands of plants and their atmospheric environment, *Q. J. R. Meteorol. Soc.*, *94*, 318–332.
- Doran, J. C., and T. W. Horst (1981), Velocity and temperature oscillations in drainage winds, *J. Appl. Meteorol.*, *20*, 360–364.
- Durran, D. R. (1990), Mountain waves and downslope winds, in *Atmospheric Processes Over Complex Terrain*, edited by B. Blumen, pp. 59–81, Am. Meteorol. Soc., Boston.
- Feigenwinter, C., C. Bernhofer, and R. Vogt (2004), The influence of advection on the short term CO₂-budget in and above a forest canopy, *Boundary Layer Meteorol.*, *113*, 201–224.
- Fleagle, R. G. (1950), A theory of air drainage, *J. Meteorol.*, *7*, 227–232.
- Fons, W. L. (1940), Influence of forest cover on wind velocity, *J. For.*, *38*, 481–486.
- Goulden, M. L., J. W. Munger, S. M. Fan, B. C. Daube, and S. C. Wofsy (1996), Measurements of carbon sequestration by long-term eddy covariance: Methods and a critical evaluation of accuracy, *Global Change Biol.*, *2*, 169–182.
- Hoener, S. F. (1965), *Fluid Dynamic Drag: Practical Information on Aerodynamic Drag and Hydrodynamic Resistance*, S. F. Hoener, Midland Park, N. J.
- Inoue, E. (1963), On the turbulent structure of air flow within crop canopies, *J. Meteorol. Soc. Jpn.*, *41*, 317–326.
- Katul, G. G., and J. D. Albertson (1998), An investigation of higher order closure models for a forested canopy, *Boundary Layer Meteorol.*, *89*, 47–74.
- Lalic, B., and D. T. Mihailovic (2002), A new approach in parameterization of momentum transport inside and above forest canopy under neutral conditions, in *Integrated Assessment and Decision Support: Proceedings of the 1st Biennial Meeting of the International Environmental Modelling and Software Society*, vol. 2, edited by A. E. Rizzoli and A. J. Jakeman, pp. 139–154, Int. Environ. Modell. and Software Soc., Manno, Switzerland.
- Landsberg, J. J., and G. B. James (1971), Wind profiles in plant canopies: Studies on an analytical model, *J. Appl. Ecol.*, *8*, 729–741.
- Lauder, B. E., and D. B. Spalding (1974), The numerical computation of turbulent flows, *Comput. Methods Appl. Mech. Eng.*, *3*, 269–289.
- Macdonald, R. W. (2000), Modelling the mean velocity profile in the urban canopy layer, *Boundary Layer Meteorol.*, *97*, 25–45.
- Mahrt, L. (1982), Momentum balance of gravity flows, *J. Atmos. Sci.*, *39*, 2701–2711.
- Mahrt, L., X. Lee, A. Black, H. Neumann, and R. M. Staebler (2000), Nocturnal mixing in a forest subcanopy, *Agric. For. Meteorol.*, *101*, 67–78.
- Mahrt, L., D. Vickers, J. Sun, N. O. Jensen, H. Jorgensen, E. Pardyjak, and H. Fernando (2001), Determination of the surface drag coefficient, *Boundary Layer Meteorol.*, *99*, 249–276.
- Manins, P. C., and B. L. Sawford (1979), A model of katabatic winds, *J. Atmos. Sci.*, *105*, 1011–1025.
- Marcolla, B., A. Cescatti, L. Montagnani, G. Manca, G. Kerschbaum, and S. Minerbi (2005), Importance of advection in the atmospheric CO₂ exchanges of an alpine forest, *Agric. For. Meteorol.*, *130*, 193–206.
- Massman, W. J. (1987), A comparative study of some mathematical models of the mean wind structure and aerodynamic drag of plant canopies, *Boundary Layer Meteorol.*, *40*, 179–197.
- Massman, W. J. (1997), An analytical one-dimensional model of momentum transfer by vegetation of arbitrary structure, *Boundary Layer Meteorol.*, *83*, 407–421.
- Massman, W. J., and J. C. Weil (1999), An analytical one-dimensional second-order closure model of turbulence statistics and the Lagrangian time scale within and above plant canopies of arbitrary structure, *Boundary Layer Meteorol.*, *91*, 81–107.
- Mohan, M., and M. K. Tiwari (2004), Study of momentum transfer within a vegetation canopy, *Proc. Indian Acad. Sci. Earth Planet. Sci.*, *113*, 67–72.
- Monson, R. K., A. A. Turnipseed, J. P. Sparks, P. C. Harley, L. E. Scott-Denton, K. L. Sparks, and T. E. Huxman (2002), Carbon sequestration in a high-elevation, subalpine forest, *Global Change Biol.*, *8*, 459–478.
- Oliver, H. R. (1971), Wind profiles in and above a forest canopy, *Q. J. R. Meteorol. Soc.*, *97*, 548–553.
- Patankar, S. V. (1980), *Numerical Heat Transfer and Fluid Flow*, 197 pp., McGraw-Hill, New York.
- Poggi, D., A. Porporato, L. Ridolfi, J. D. Albertson, and G. G. Katul (2004), The effect of vegetation density on canopy sub-layer turbulence, *Boundary Layer Meteorol.*, *111*, 565–587.
- Raupach, M. R., and R. H. Shaw (1982), Averaging procedures for flow within vegetation canopies, *Boundary Layer Meteorol.*, *22*, 79–90.
- Raupach, M. R., and P. G. Thom (1981), Turbulence in and above plant canopies, *Annu. Rev. Fluid Mech.*, *13*, 97–129.
- Raupach, M. R., P. A. Coppin, and B. J. Legg (1986), Experiments on scalar dispersion within a plant canopy, part I: The turbulence structure, *Boundary Layer Meteorol.*, *35*, 21–52.
- Schimmel, D. S., T. G. F. Kittel, S. Running, R. K. Monson, A. A. Turnipseed, and D. Anderson (2002), Carbon sequestration studied in western US mountains, *Eos Trans. AGU*, *83*, 445, 449.
- Shaw, R. H. (1977), Secondary wind speed maxima inside plant canopies, *J. Appl. Meteorol.*, *16*, 514–521.
- Shaw, R. H., R. H. Silversides, and G. W. Thurtell (1974), Measurements of mean wind flow and three-dimensional turbulence intensity within a mature corn canopy, *Agric. Meteorol.*, *13*, 417–425.

- Siqueira, M., and G. G. Katul (2002), Estimating heat sources and fluxes in thermally stratified canopy flows using higher-order closure models, *Boundary Layer Meteorol.*, *103*, 125–142.
- Staebler, R. M., and D. R. Fitzjarrald (2004), Observing subcanopy CO₂ advection, *Agric. For. Meteorol.*, *122*, 139–156.
- Thom, A. S. (1971), Momentum absorption by vegetation, *Q. J. R. Meteorol. Soc.*, *97*, 414–428.
- Turnipseed, A. A., D. E. Anderson, P. Blanken, and R. K. Monson (2002), Energy balance above a high-elevation subalpine forest in complex topography, *Agric. For. Meteorol.*, *110*, 177–201.
- Turnipseed, A. A., D. E. Anderson, P. D. Blanken, W. M. Baugh, and R. K. Monson (2003), Airflows and turbulent flux measurements in mountainous terrain. Part 1. Canopy and local effects, *Agric. For. Meteorol.*, *119*, 1–21.
- Turnipseed, A. A., D. E. Anderson, S. Burns, P. D. Blanken, and R. K. Monson (2004), Airflows and turbulent flux measurements in mountainous terrain. Part 2. Mesoscale effects, *Agric. For. Meteorol.*, *125*, 187–205.
- Wilson, J. D., D. P. Ward, G. W. Thurtell, and G. E. Kidd (1982), Statistics of atmospheric turbulence within and above a corn canopy, *Boundary Layer Meteorol.*, *24*, 495–519.
- Wilson, N. R., and R. H. Shaw (1977), A higher order closure model for canopy flow, *J. Appl. Meteorol.*, *16*, 1197–1205.
- Yakhot, V., S. A. Orzag, S. Thangam, T. B. Gatski, and C. G. Speziak (1992), Development of turbulence models for shear flows by a double expansion technique, *Phys. Fluids A*, *4*, 1510–1520.
- Yi, C., K. J. Davis, P. S. Bakwin, B. W. Berger, and L. Marr (2000), The influence of advection on measurements of the net ecosystem-atmosphere exchange of CO₂ from a very tall tower, *J. Geophys. Res.*, *105*, 9991–9999.
-
- G. Allwine and B. Lamb, Laboratory for Atmospheric Research, Washington State University, Pullman, WA 99164-2910, USA.
- D. E. Anderson, Water Resources Discipline, U.S. Geological Survey, Denver Federal Center, Lakewood, CO 80225, USA.
- S. P. Burns, R. K. Monson, and C. Yi, Department of Ecology and Evolutionary Biology, University of Colorado, Boulder, CO 80309-0334, USA. (yic@colorado.edu)
- A. A. Turnipseed, Atmospheric Chemistry Division, National Center for Atmospheric Research, Boulder, CO 80305, USA.
- Z. Zhai, Department of Civil, Environmental, and Architectural Engineering, University of Colorado, Boulder, CO 80309-0428, USA.